AIAA JOURNAL
Vol. 32, No. 4, April 1994

Heat Transfer Measurements and Computations of Swept-Shock-Wave/Boundary-Layer Interactions

Y. Lee* and G. S. Settles†
Pennsylvania State University, University Park, Pennsylvania 16802
and
C. C. Horstman‡
NASA Ames Research Center, Moffett Field, California 94035

An experimental and computational research program providing new knowledge of the heat transfer in swept-shock-wave/boundary-layer interactions is described. An equilibrium turbulent boundary layer on a flat plate is subjected to impingement by a swept planar shock wave generated by a sharp fin. Five different interactions with fin angles ranging from 10 to 20 deg at freestream Mach numbers of 3 and 4 produce a variety of interaction strengths ranging from weak to very strong. A foil heater generates a uniform heat flux over the flat plate surface, and miniature thin-film-resistance sensors are used to measure the local surface temperature. The heat convection equation is then solved for the heat transfer distribution within an interaction, yielding an uncertainty of about ±10%. These data are compared with numerical Navier-Stokes solutions that employ a k-ε turbulence model. A simple peak heat transfer correlation for fin interactions is suggested.

Introduction

THE study of shock-wave/turbulent-boundary-layer interactions is important for the solution of internal and external aerodynamic problems in the design of high-speed vehicles, as well as for the validation of the associated numerical simulations. Despite many previous studies of the overall problem, little knowledge has been gained of swept interactions until quite recently, and more extensive experimental work is still needed for a better understanding of the dynamics of such flows.

When an oblique shock wave of sufficient strength impinges upon a solid surface and interacts with the turbulent boundary layer on that surface, a three-dimensional separated region is generated there. Peak values of surface pressure, skin friction, and heat transfer are then observed to occur near the attachment line of this separated flow. These peak values are of great practical importance in establishing the limits of mean aerothermal loads on high-speed flight vehicles. Also, turbulence and unsteady shock motion result in fluctuations of pressure, skin friction, and heat transfer in such flows, which are sources of serious additional aerothermal loads of an unsteady nature.

With the advent of supercomputers, the computation of such three-dimensional shock/boundary-layer interactions has recently become feasible. Extensive computational fluid dynamics (CFD) studies of sharp-fin-generated swept interactions have been conducted by Horstman,[1] Knight,[2,3] Knight and Badekas,[4] and Knight et al.[5] for various interaction strengths using several different turbulence models. These computational results can predict surface pressure distributions and the gross features of the flowfields reasonably well. However, it is known that the prediction of surface pressures is not a definitive test of the turbulence modeling employed in these CFD codes. A more definitive test requires that the gradient transport of heat and momentum at the surface be predicted as well. Accurate experimental measurements of skin friction and heat transfer distributions are therefore important for this purpose. Unfortunately, such data of sufficiently high quality and quantity have not generally been available in swept-shock/boundary-layer interactions.

The present experimental program has been designed to provide new "benchmark" data of the type required for turbulence modeling, code validation, and physical understanding of these swept interactions. The heat transfer distributions beneath a range of swept interactions are measured, analyzed, and compared with CFD predictions. However, the measurement of accurate, high-spatial-resolution, steady-state heat transfer distributions in swept interactions in a near-adiabatic wind tunnel has first required the development of a novel experimental technique, which is also described later.

Literature Review

Reviews by Settles and Dolling[6,7] cover the progress of research on the swept interaction problem up to 1990. Many studies of the surface properties of such interactions have been made. Some of the more recent of these[8,9] include both surface pressure and skin friction data. Along with these measurements, detailed nonintrusive flowfield studies[10,11] have clarified some previous questions about swept interaction physics.

In 1977 Neumann and Hayes[12] proposed an empirical correlation for the peak aerodynamic heating in sharp-fin-generated swept interactions. Holden[13] then correlated the results of a number of swept interaction heat transfer experiments with the peak surface-pressure ratio in 1984. Both studies showed that high localized heat transfer occurs near the junction of the fin and the surface. In 1987, Hayashi et al.[14] measured heat transfer distributions in swept interactions using a newly developed thin-film gauge. Most recently, Rodi and Dolling[15] measured the surface heat transfer distributions in swept interactions at Mach 5 using steady-state thermopile-type "Schmidt-Boelter" gauges. General references[16-19] are available on these conventional heat transfer measurement techniques and instruments. Only the technique of present interest is discussed further here.

Thin-Film Gauges

The development of evaporated metallic-film coating technology in other fields has spawned thin-film gauges that are

Presented as Paper 92-3665 at the AIAA/SAE/ASME/ASEE 28th Joint Propulsion Conference, Nashville, TN, July 6–8, 1992; received Sept. 9, 1992; revision received Sept. 18, 1993; accepted for publication Sept. 21, 1993.

*Graduate Student, Mechanical Engineering Department.
†Professor, Mechanical Engineering Department, and Director, Gas Dynamics Laboratory.
‡Senior Scientist (Retired), Experimental Fluid Dynamics Branch.

becoming widely used in aerodynamic testing. Because of its high sensitivity and fast response, the thin-film gauge is applied in a variety of ways. It can measure highly transient surface temperatures, it can be used as a calorimeter gauge, or it can constitute the sensing element in a multilayer "sandwich" gauge. Epstein et al.[20] used such gauges to measure the heat flux to a transonic turbine, whereas Hayashi et al.[14] first used them to measure heat flux in a shock/boundary-layer interaction. Thin-film gauges have also been used in transition detection studies (e.g., Johnson et al.[21]).

Although the thin-film technique has versatility, accuracy, and fast response, its fabrication by microlithographic techniques is expensive. The resulting thin-film sensors also need care in handling, annealing to prevent drift, and highly accurate calibration procedures.

Resistance Heater Methods

For heat transfer measurements in "cold" facilities, it is apparent that external heating or cooling is needed, since a sufficient difference between the surface temperature and the adiabatic wall temperature is critical to the signal-to-noise ratio of the measurement. Such is the case in the present study. Though cooling by way of a circulated refrigerant has been attempted in the past, we have chosen heating by an embedded resistance heater as the simplest means to vary the surface temperature.

The resistance heater method is the most widely used technique to apply external heating for steady-state heat flux measurements. A heating element inside the surface of a test model generates enough heat to raise the surface temperature significantly. During a test the electrical power input to the heater equals the convective heat transfer from the model surface at steady state. By measuring the local surface temperature and applying the heat convection equation, one can calculate the heat transfer coefficient.

For example, Simonich and Moffat[22] used a thin gold-film resistance heater to generate a heat flux and liquid crystals to sense the resulting surface temperature distribution. Hippensteele et al.[23] evaluated commercially available elements for use in the resistance-heater technique. Abuaf et al.[24] used a resistance-heater/liquid-crystal combination to measure heat transfer in a jet impingement experiment. Eibeck and Eaton[25] used thermocouple measurements beneath a foil heater to investigate the heat transfer effect of a longitudinal vortex in a turbulent boundary layer.

These methods, however, have been used only for relatively low-speed flows so far. Higher heat generation rates and accurate multipoint surface temperature measurements are needed in high-speed flows. In this study we attempt to combine the aforementioned heat transfer methods to obtain a high-resolution, steady-state measurement technique for high-speed flow in a near-adiabatic wind-tunnel facility. Further, to obtain high-spatial-resolution data with a modest number of discrete gauges, the inherent symmetry of swept interactions must be exploited as well.

Quasiconical Interaction Structure

The salient feature of the swept sharp-fin interaction (see Fig. 1) is its quasiconical symmetry. This has been observed by many investigators and recently confirmed by parametric studies.[8,10] The spanwise interaction growth is found to be essentially conical except for an initial "inception zone" in the vicinity of the fin leading edge. The surface features of this quasiconical interaction appear to emanate from a single point, which has been termed the "virtual conical origin" (VCO). Thus a projection along the conical rays of the interaction from the VCO onto the unit sphere reduces the problem to two dimensions, which is a powerful simplification.[7]

Such projections, or flowfield maps, are shown in Ref. 10 for the interaction structure in angular coordinates ϕ and β. The swept interaction is seen to consist of a main (inviscid) shock wave that bifurcates into a λ foot supported by a separation vortex. The streamtube processed by the λ foot turns downward and impinges upon the flat plate at the rear of the interaction. Though quasiconicity is not a flawless representation of swept interactions, it nonetheless provides a "natural" framework for the engineering analysis of such flows.

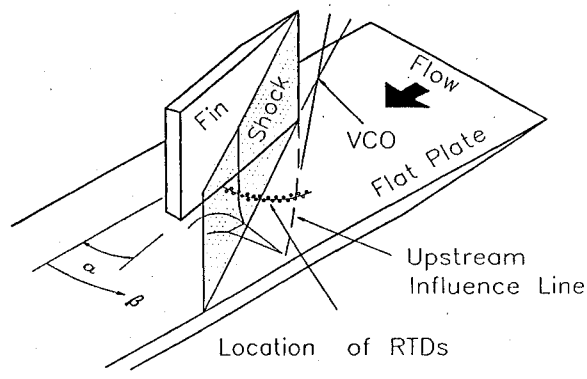

Fig. 1 Sketch of test geometry.

Experimental Methods

Wind-Tunnel Facility and Test Conditions

The experiments were performed in the Penn State Gasdynamics Laboratory's supersonic wind-tunnel facility, which is an intermittent blowdown tunnel with a test section size of 15 × 17 × 60 cm. The facility has a unique variable Mach number capability over the range of Mach 1.5 to 4.0 by way of an asymmetric sliding-block nozzle. A 57-m^3 20-atm pressure reservoir provides testing times up to 2 min at stagnation pressures up to 15 atm and a near-ambient stagnation temperature. The experiments described in this paper were performed at nominal freestream Mach numbers of 3 and 4, with corresponding unit Reynolds numbers of 6.8 and 7.0 × 10^7/m, respectively.

Fin Shock Generator

The interaction is generated by an equilibrium, adiabatic flat plate boundary layer interacting with the swept, planar oblique shock wave generated by an upright, sharp leading-edge fin at an angle of attack (see Fig. 1). The fin leading edge is 21.6 cm aft of the plate leading edge. The size of the fin is small enough to avoid blockage of the flow but large enough to generate a "dimensionless semi-infinite" interaction on the flat plate (see Settles and Dolling[6]).

Turbulent Boundary Layer

Natural boundary-layer transition typically occurs within 1–2 cm of the flat-plate leading edge at the present high Reynolds numbers. Pitot surveys and a wall-wake analysis have established that the flat-plate boundary layer is both two dimensional and in turbulent equilibrium for the range of present test conditions. The parameters of the boundary-layer profile at a position 17.8 cm downstream of the flat-plate leading edge and on the plate centerline are taken as the upstream boundary condition for the present experiments. At freestream Mach numbers 3 and 4, respectively, the boundary-layer thickness is 2.7 and 2.9 mm, the displacement thickness is 0.8 and 1.0 mm, and the momentum thickness is 0.17 and 0.13 mm. A more complete documentation of the test boundary layers may be found in Lu.[8]

The turbulent boundary layer is naturally near adiabatic (the ratio of the wall temperature T_w to the adiabatic wall temperature T_{aw} is typically 1.03). The resultant thermal potential is small, thus requiring special means to make heat transfer measurements.

Flat Plate for Heat Transfer Measurements

The flat plate for heat transfer measurements, diagrammed in Fig. 2, is a "sandwich" consisting of a top sheet of resistance

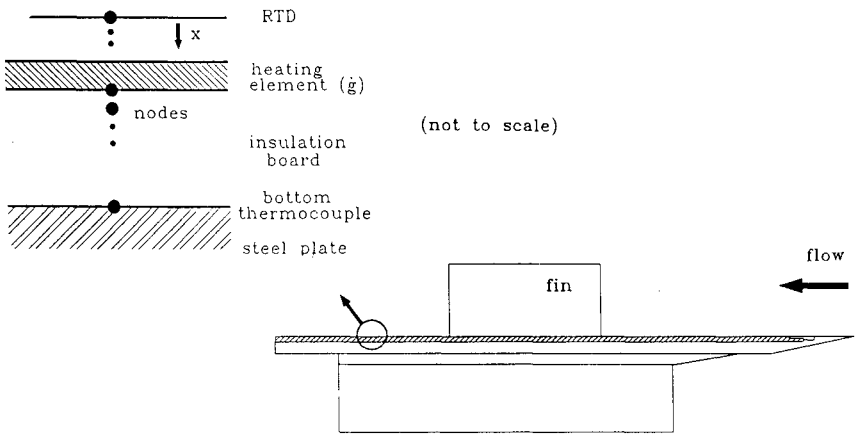

Fig. 2 Sketch of multilayer construction of flat plate.

temperature detector (RTD) sensors, a foil heater, an insulation board, and a stainless steel supporting plate. A few thermocouples are also distributed inside the insulation board. Heat is generated by the foil heater, and the surface temperature distribution is measured by the RTD sensors. The heat convected to the flow in steady state equals the total heat generated by the heater (V^2/R) minus the heat loss through the insulation board. However, the adiabatic wall temperature is also needed in the calculation of a heat transfer coefficient and is indirectly measured as described later.

RTD Surface Temperature Sensors

Custom-made thin-film RTD sensors were vacuum deposited on a plastic substrate using microlithographic fabrication techniques. These thin-film sensors can measure T_w accurately without disruption of the flow. They also have a high frequency response, though only steady-state data are considered in this paper.

Each of the 37 RTD sensors consists of a nickel-film resistance thermometer of about 1000-Å thickness deposited on the 50-μm-thick Kapton polyimide substrate sheet. The sheet itself is then attached to the flat surface of the foil heater using laminating epoxy cement. Nickel is chosen as the sensing element because of its relatively high sensitivity and its excellent adhesion characteristics in thin-film applications. The sensor geometry is a square 1 × 1 mm serpentine pattern. This pattern maximizes the sensor length in a small surface area, thus producing a high room temperature resistance (65 Ω), a high signal-to-noise ratio, and effectively a "point" surface temperature measurement. Low-resistance 6-μm-thick copper-film leads are also deposited from each sensor to the edge of the polyimide sheet. These leads are individually soldered to a 37-conductor coaxial cable, which is then connected to a specially designed 37-channel signal conditioner outside the test section.

To utilize the conical nature of the fin interaction, a double-circular-arc distribution of the 37 temperature sensors (at radii of 86.4 and 91.4 mm from the fin leading edge) is chosen, as shown schematically in Fig. 1. In terms of the angle β, defined in Fig. 1, these gauges are spaced at a 2-deg angular separation from β = 6 to 78 deg with respect to the freestream for high data resolution.

Heater

Two types of heating methods are commercially available: surface resistance heaters and the radiation method. The latter utilizes external lamps focused on the model and is generally a costly and difficult technique. Surface resistance heaters, on the other hand, are widely used because of their relatively low cost and easy application. In this method, the model is heated by a resistance foil imbedded in the model surface.

There are four major requirements for the heater in the present experiment. 1) High heat flux is required due to the large convective heat transfer expected in high-speed flows. 2) The heat flux should be uniform over the surface of interest. 3) For quick heating during a typical wind-tunnel run of about 30 s, the thermal mass of the heater should be small. 4) The surface of the heater should be flat and smooth, since the RTD sheet is mounted upon it and exposed to the flow.

Commercially manufactured "unetched-foil" heaters, as used in a variety of experiments,[22-25] showed quite satisfactory results in terms of uniform heat flux and easy application. However, all of these heaters were found to be unsuitable for present purposes because their resistances were too low to generate sufficient heat flux in practice.

For the present study, an Inconel "etched-foil" heater was used instead. This heater is thin and flexible, consisting of an etched-foil resistive element laminated between layers of flexible insulation. It also has a thin aluminum foil over the top surface of the heating element to enhance uniform heating. Custom-made by Minco Products, Inc., it is 0.25 mm thick and its room temperature resistance is 21.6 Ω. Using laminating epoxy cement, it is sandwiched between the RTD sheet and the insulation board (see Fig. 2).

Insulation Board

The heat generated by the heater is transferred to the surroundings by conduction, convection, and radiation. In the present experiment, radiation is negligible because the temperature is near ambient. Thus a portion of the heat energy is assumed to be convected to the flow over the plate, whereas the remainder is conducted through the insulation board underlying the heater. A good insulator is needed to minimize this conduction loss. The insulator should further be rigid enough to support the heater during exposure to high-shear flows and should be machined for surface flatness.

"Rexolite" plastic was chosen for this purpose. It has a low thermal conductivity (0.00035 cal/s/cm/°C) and also satisfies the stated mechanical requirements. A 4.76-mm-thick "Rexolite 1422" sheet was purchased from Almac Plastic Corp. and was machined to size. After attaching the heater and RTD sheet to the insulation board using a "vacuum bagging" technique,[26] we installed the entire assembly on the stainless steel flat plate. Also, to measure the temperature change of the insulation board, we installed three quick-response thermocouples on its top face and two on its bottom face.

Instrumentation

The RTD sensors, which are at the heart of this experiment, measure temperature by the change of resistance of a sensor according to a prior calibration. To measure the resistance, it is necessary to provide a constant current flow to the RTD. A signal-conditioning instrument was fabricated for this purpose, consisting of 37 sets of constant-current sources (1.5 mA), amplifiers, and low-pass filters for each of the 37 RTD channels.

For the calibration of the RTDs, the internal heater of the plate and a precision thermocouple are used. The heater elevates the temperature of the RTDs, and this temperature is measured by the thermocouple. To maintain a uniform temperature over all sensors, a large aluminum block in which the thermocouple is installed is placed on top of the plate, and the assembly is allowed to reach thermal equilibrium before data are read.

The foil heater is powered through wires connected to an ac variable transformer that has an output voltage up to 280 V and a current up to 15 A. The voltage applied to the heater is recorded during testing.

Data Acquisition

A LeCroy waveform recorder controlled by a 386-class microcomputer is used for data acquisition. It has 12 channels of high-speed data sampling capability at rates up to 5 Mhz and 32 channels of relatively low-speed data sampling at rates up to 5 Khz. All of these channels utilize 12-bit digitization. The "ASYST" software package is employed for data handling. During experiments, signals from the RTD sensors and thermocouples of the heat transfer model, as well as signals from the wind-tunnel stilling chamber, are all simultaneously recorded on the LeCroy system.

Data Reduction

The present heat transfer measurement technique requires an accurate determination of all of the terms in the definition of the Stanton number C_h:

$$C_h = \frac{h}{\rho_\infty V_\infty c_p} = \frac{q''_{\text{conv}}}{\rho_\infty V_\infty c_p (T_w - T_{aw})} \tag{1}$$

where h is the convective heat transfer coefficient; ρ_∞, V_∞, c_p are the freestream density, velocity, and specific heat, respectively; and q''_{conv} (W/m^2) is the heat convected to the flow.

Except for T_w, which is directly measured by the RTD sensors, all terms in the previous equation must be found indirectly from measured values. In particular, the accuracy of both q''_{conv} and T_{aw} is essential, since these terms principally determine the accuracy of the Stanton number. However, they are not easy to measure; T_{aw} is never reached during the present brief wind-tunnel runs, even on an insulating model. Further, the variation of temperature within the insulation board is complex during a run due to changing stagnation temperature and heater voltage, requiring that a special calculation be performed.

Calculation of Heat Convected to Flow

From the measured voltage applied to the foil heater and its resistance, its heat efflux is easily calculated. However, not all of this heat is convected to the flow. There is also a conduction loss through the insulation board that must be determined. It is calculated using the measured RTD temperature and the bottom temperature of the insulation board by solving the time-dependent one-dimensional heat diffusion equation with an imbedded heat-source layer:

$$\frac{\partial T}{\partial t} = \frac{\partial}{\partial x}\left(D \frac{\partial T}{\partial x}\right) + \rho c_p \dot{g} \tag{2}$$

where t is time; x is the depth into the plate measured normal to the top surface of the RTD sheet (see Fig. 2); and D, ρ, and c_p are the thermal diffusivity, density, and specific heat of the multilayered components of the plate, respectively. Also, $\dot{g}$ (W/m^3) is the rate at which heat is generated per unit volume of the foil heater. The measured time-dependent RTD and insulator-bottom temperatures serve as boundary conditions, and a constant-temperature initial condition throughout the plate is both assumed in the solution and forced in the actual experiment by allowing adequate time for thermal equilibration between runs. The numerical solution of Eq. (2) yields temperature vs time for 49 nodes within the plate, from which the time-dependent conduction loss to the insulation board, q''_{loss} (W/m^2), is obtained from Fourier's law:

$$q''_{\text{loss}} = -k \frac{dT}{dx} \tag{3}$$

using the first two node temperatures at the top of the insulation board to form the gradient (k is the thermal conductivity of the insulation board).

In steady state, q''_{conv} is then calculated by subtracting this conduction loss from the heat efflux of the heater. However, possible thermal transients in the heater and RTD sheet require that q''_{conv} actually be calculated by Fourier's law as well, using the first two nodes directly beneath the surface of the RTD sheet to form the gradient.

Of course, the previous procedure accounts only for conduction normal to the plate surface. Lateral conduction effects are estimated in Ref. 26 and found to be, at worst, 20–30% of the normal conduction, which is itself on the order of 10% of the total heater output. Accordingly, no correction has been carried out for lateral conduction.

Adiabatic Wall Temperature

In the present experiment an accurate evaluation of T_{aw} is a most critical step, since $T_w - T_{aw}$ is relatively small at the location of peak heat transfer in the shock/boundary-layer interaction. Although most previous experimental studies have assumed that T_{aw} is constant beneath such interactions, it is necessary to check that assumption here to maintain the accuracy of the present results.

There are two methods generally used to measure T_{aw}: the "direct" method and the "indirect" or extrapolation method. The direct method measures T_{aw} directly on an insulated model after thermal equilibrium is reached.[27–29] However, in most of these cases the required tunnel run time would be quite long, which is not possible for the present tests.

Neumann and Hayes[12] discuss the general problem of recovery temperature (T_{aw}) measurement and present an elegant way to solve it. This method involves making several heat flux measurements at different wall temperatures. Since the heat flux is linear with T_w so long as the heat convection coefficient is constant, a linear fit to the data can be extrapolated to the temperature at which zero heat is convected to the flow, which is identically T_{aw}. The present experiments employ this indirect method.

Error Analysis

The uncertainty of each variable in the data reduction process contributes to the uncertainty of the final result. As Coleman and Steele[30] suggest, the total uncertainty of the present measurements is determined by calculating and combining the "root-sum-squares" of the uncertainties of each variable. This calculation indicates a maximum total uncertainty in C_h of about $\pm 10\%$ for all five present interaction cases. This accuracy level is believed to qualify the present results as "benchmark" data for code validation and turbulence modeling purposes. The error bars shown on selected points in the upcoming figures reflect this uncertainty estimate.

Computational Methods

The governing equations describing the shock/boundary-layer interaction flowfield are the compressible three-dimensional Navier-Stokes equations using mass-averaged variables in strong conservation form.[31] Their restrictions include the calorically perfect-gas assumption, the Sutherland viscosity law, and zero bulk viscosity. Turbulence closure is achieved with a two-equation eddy-viscosity (k-ε) model using the Jones-Launder low-Reynolds-number terms.[32] This model was chosen over other available models for its potentially greater

range of applicability (since it does not require the prescription of a length scale), and because it has become more commonly used by the aerospace industry. Further details of the boundary conditions and algorithm used here are given by Knight et al.[33] and Horstman.[1]

The computations employ the full three-dimensional equations rather than a conical simplification because the viscous surface properties (e.g., heat transfer) are not assumed a priori to follow the quasiconical behavior of the inviscid flowfield. Further discussion of this issue and comparisons between three-dimensional and conical swept interaction solutions are found in Ref. 34.

The grid adequately resolves the flowfield and meets all of the criteria for grid resolution employed in previous three-dimensional turbulent interaction studies.[1,5,9,33,34] The grid spacing near the wall was shown to be adequate for predicting the heat transfer in a previous study[35] wherein a grid refinement was performed.

The computational domain extends from an upstream boundary where an equilibrium turbulent boundary layer is generated (matching the experimental data) to a point well downstream of the interaction. Within this domain the grid is generated so as to take advantage of the experimentally observed quasiconical flowfield. In the x-z (horizontal) plane the grid utilizes a family of rays originating at the fin leading edge. Ahead of the interaction these rays are replaced by lines of constant z (spanwise direction). In the x (streamwise) direction, constant spacing is used. In the y (vertical) direction a variable spacing is used, concentrating most of the points within the boundary layer. The maximum value of y^+ for the first grid point is 0.1 within the interaction. The resulting grid spacing in the x and z directions is about half the incoming boundary-layer thickness. The total computational domain involves 64 × 40 × 64 grid points in the x, y, and z directions, respectively.

The choice of radial grid origin at the fin leading edge is a simplification in both the experiments and computations, since the VCO of the experiment always lies a short distance ahead of the leading edge. The angular coordinate β is accurate to better than ±2 deg in both cases. See Ref. 34 for a discussion of the choice of VCO location.

To calculate C_h, two separate computations are made for each test case. The heat convected to the flow is determined from the first computation, in which T_w is set at 22°C above the stagnation temperature. A second computation is then made to find T_{aw}, where the heat convected to the flow is set to zero as a boundary condition. The variable C_h is then calculated using Eq. (1), just as in the case of the experimental data. Ideally, in fact, six computations should be done, just as six experiments are carried out at different heating rates, for better accuracy. However, since each solution requires 25 h on the NASA Ames Cray Y-MP supercomputer, such an approach is not realistic. For one case, however, a third solution was obtained for a second value of wall temperature. The heat transfer coefficient was then calculated three ways using each pairing of the solutions. Each of these three calculated distributions varied by a maximum of only 5% from their average value.

Results and Discussion

Figure 3 shows the time variations of T_w at two representative RTD sensor locations (β = 64 deg, located outside the interaction, and β = 20.8 deg, located at the point of peak heat transfer) in the Mach 4, α = 16 deg fin interaction without heating. Figure 4 shows the corresponding case with heating, where the two wall temperatures are elevated well above the adiabatic wall temperature. The "knees" in the variation of the wall temperatures in Fig. 4 (at 12.5 s) are due to a deliberately abrupt change of the heating rate during the run, which was required to raise the plate temperature rapidly at the beginning of the run to save testing time. The tunnel stagnation and adiabatic wall temperature variations (calculated

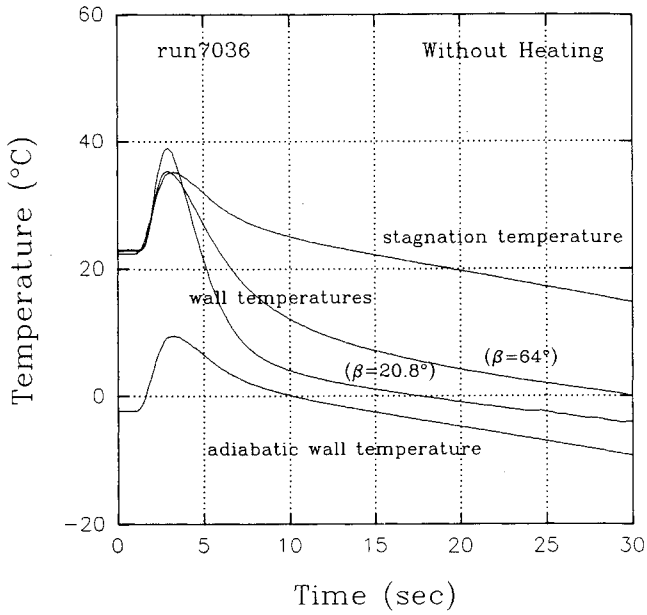

Fig. 3 Temperature variations without heating (Mach 4 and α = 16 deg).

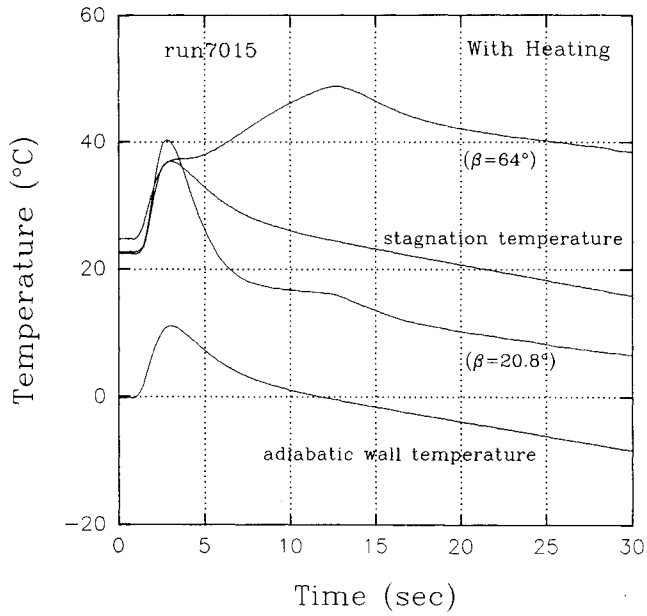

Fig. 4 Temperature variations with heating (Mach 4 and α = 16 deg).

under the assumption that the recovery factor equals 0.89 based on many measurements of high-speed turbulent boundary layers) are also shown for a comparison.

In Fig. 5 the calculation of the adiabatic wall temperature using the indirect extrapolation method described earlier is illustrated for the case of a sensor located in the flat-plate boundary layer at M_∞ = 4.0. Six different heating rates show the expected linear variation with wall temperature that, upon extrapolation, yields a flat-plate recovery factor of 0.93. A 95% confidence interval is also shown on the data in Fig. 5, which is typical of the present T_{aw} determinations and is used for the error analysis[26,30] of the measurements.

To check the accuracy of the present heat transfer technique, we carried out a comparison of the experimental results for the flat-plate case with a numerical calculation using an eddy-viscosity boundary-layer code.[36] The results show that the raw $C_{h\infty}$ data from the experiments generally agree with the CFD calculation within 15% except at certain particular RTD locations. These exceptions, at which fixed errors arise

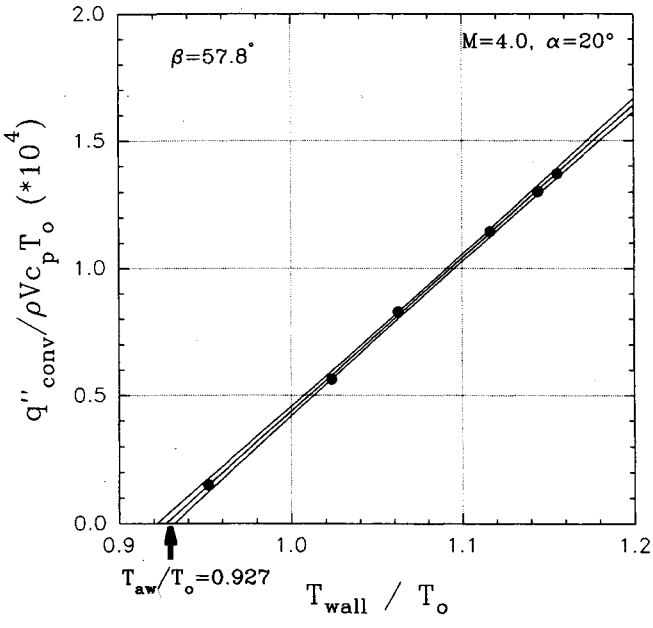

Fig. 5 Example determination of adiabatic wall temperature.

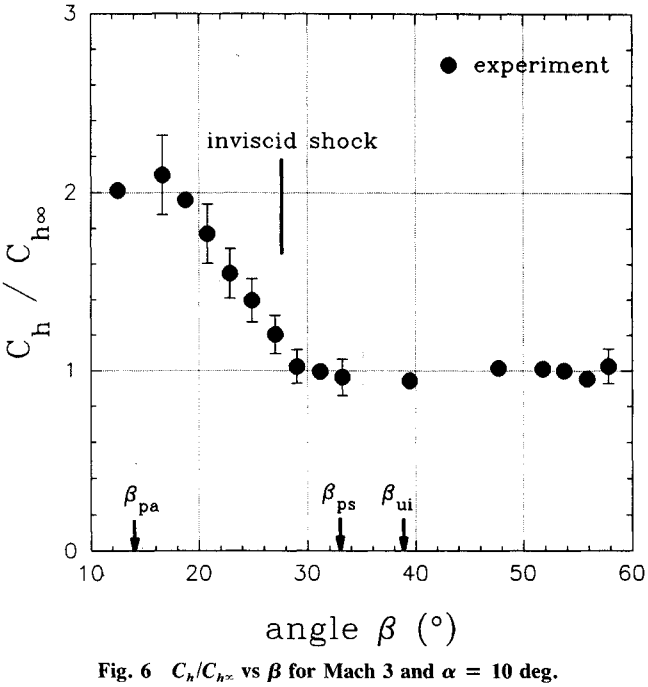

Fig. 6 $C_h/C_{h\infty}$ vs β for Mach 3 and α = 10 deg.

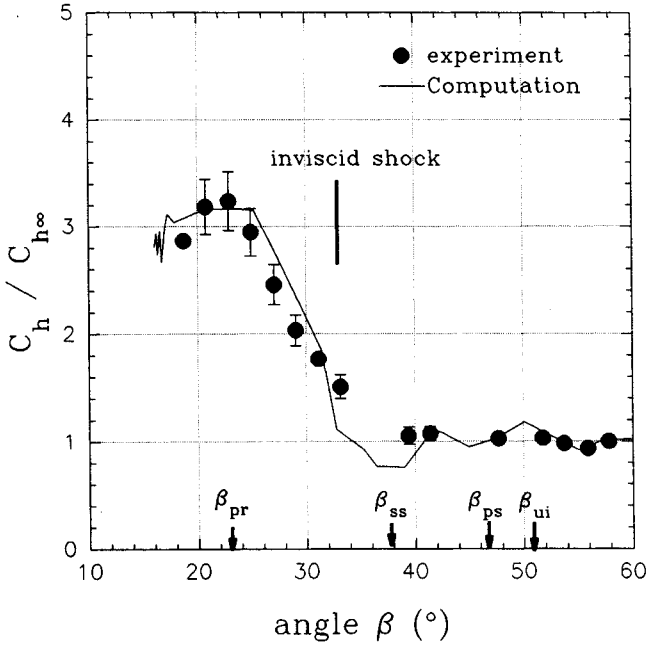

Fig. 7 $C_h/C_{h\infty}$ vs β for Mach 3 and α = 16 deg.

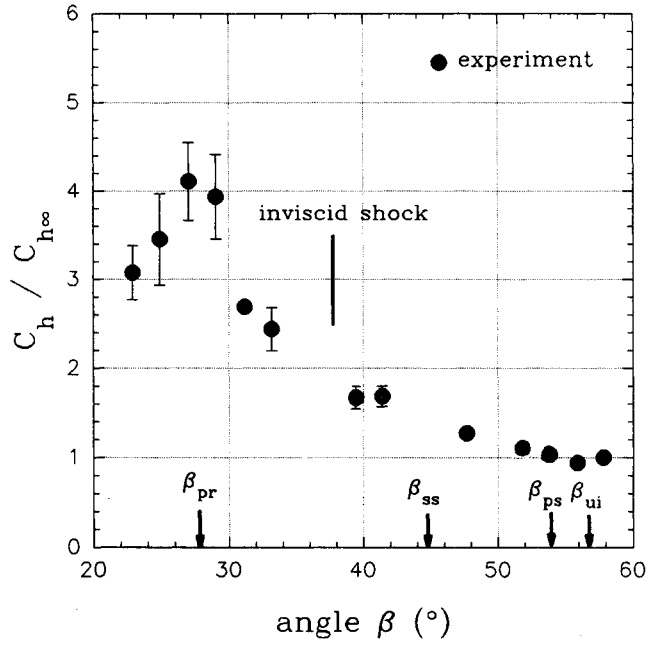

Fig. 8 $C_h/C_{h\infty}$ vs β for Mach 3 and α = 20 deg.

due to a slight local nonuniformity of the foil heater, are corrected by calibration. The $C_{h\infty}$ values that characterize the present Mach 3 and 4 experiments are 0.00086 and 0.00065, respectively.

Heat Transfer Distributions

Figures 6–10 show the normalized heat transfer distributions $C_h/C_{h\infty}$ vs the angle β for five different swept-shock-wave/boundary-layer interactions ranging from weak to strong. Here, β_{pr}, β_{ss}, β_{ps}, and β_{ui} represent the angular locations of primary attachment, secondary separation, primary separation, and upstream influence, respectively, in coordinates centered at the fin leading edge for simplicity. For the cases of M_∞ = 3.0 and α = 16 deg, and M_∞ = 4.0 and α = 16 and 20 deg, CFD solutions are also available and are shown along with the data.

The spatial fluctuations seen in the heat transfer computations are due to small differences in the level of convergence between the two solutions that must be differenced to obtain the heat transfer coefficient. (Any small oscillation in either solution will thus be greatly magnified.) The variable named $C_{h\infty}$ denotes both the flat-plate value of the experimental heat transfer and the computed flat-plate value.

The weakest interaction, M_∞ = 3.0 and α = 10 deg, shown in Fig. 6, displays a relatively featureless rise in heat transfer from the primary flow separation line to a peak at the primary attachment line, where C_h reaches about twice its flat-plate value. In the case of M_∞ = 3.0 and α = 16 deg in Fig. 7, similar features are seen, though the rise now begins at the secondary separation line and reaches a peak of $C_h/C_{h\infty}$ = 3.2. The CFD solution in this case is in very good agreement with the experimental data except in the vicinity of β_{ss}, where a "dip" below the flat-plate level is predicted but not observed in the data.

Figure 8 next shows the measured heat transfer distribution for the interaction at M_∞ = 3.0 and α = 20 deg. The rise begins at primary separation, as before, and then continues rather monotonically to a maximum at the primary attachment

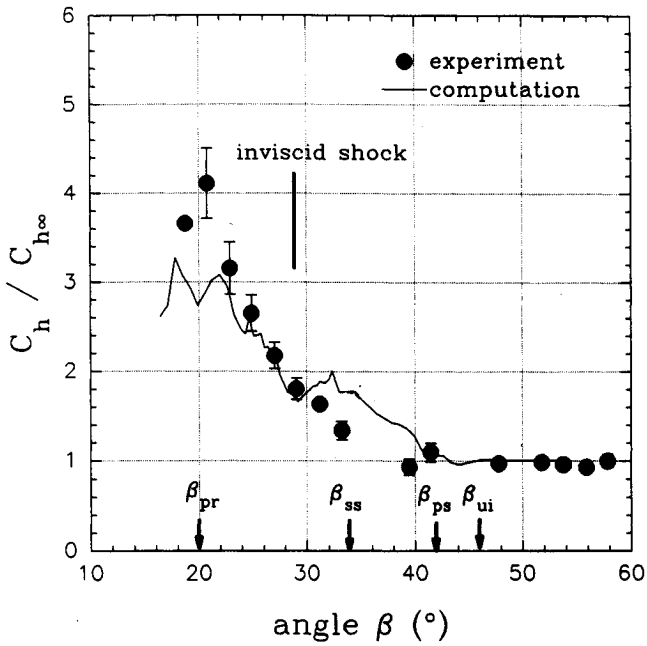

Fig. 9 $C_h/C_{h\infty}$ vs β for Mach 4 and α = 16 deg.

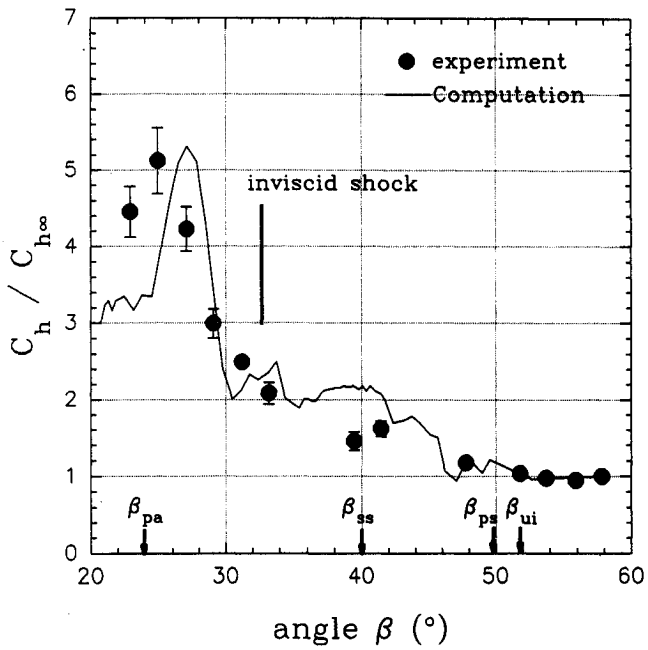

Fig. 10 $C_h/C_{h\infty}$ vs β for Mach 4 and α = 20 deg.

line, where four times the flat-plate heat transfer level is observed.

Figure 9, for the interaction at M_∞ = 4.0 and α = 16 deg, shows a case of very similar interaction strength, since the Mach number normal to the undisturbed oblique shock wave in these two cases is 1.8 and 1.9, respectively. Indeed, the observed peak heat transfer levels in Figs. 8 and 9 are almost the same. However, in the latter case the CFD solution underestimates the peak level by some 20% for unknown reasons.

Finally, Fig. 10 shows the results of the strongest interaction tested here: M_∞ = 4.0 and α = 20 deg. As in Fig. 8, a small local maximum in heat transfer is seen in the vicinity of β_{ss}. Otherwise the data rise to a peak value of $C_h/C_{h\infty}$ = 5.1 at the primary attachment line. This level is well predicted by the CFD solution, although its β location is offset slightly, because the computed boundary layer on the fin itself is too thick.

In summary, the salient feature of the present results is that peak heating occurs on the primary attachment line of these

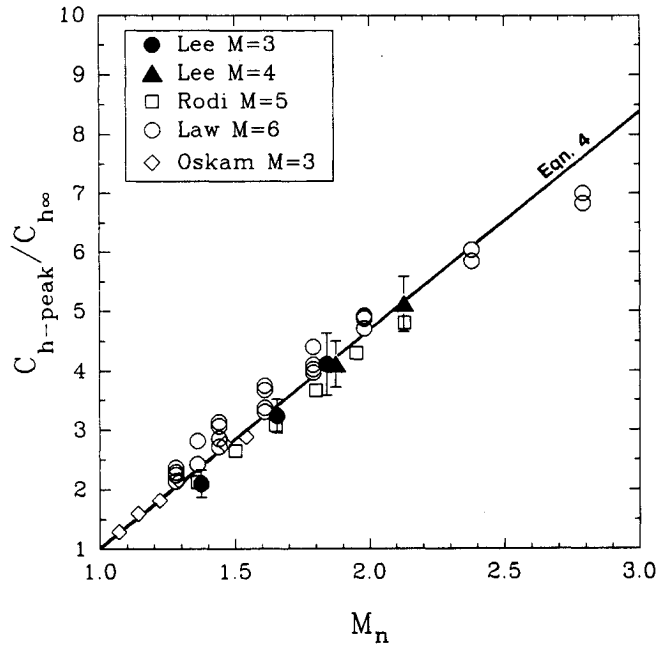

Fig. 11 New peak heating correlation.

swept interactions. The peak heating level also rises monotonically with normal Mach number M_n (a first-order interaction strength parameter[10]), as shown by both the experimental data and the CFD solutions.

Peak Heating Correlation

The peak heating correlation of Neumann and Hayes[12] is a function of both M_n and position x/δ downstream of the fin leading edge. Their work was done before the quasiconical nature of the fin interaction was generally recognized. If it is assumed that C_h asymptotes to a constant value along a conical ray outside the interaction inception zone, as is shown experimentally by Rodi and Dolling,[15] then a much simpler data correlation can be posed in terms of $C_{h_{peak}}/C_{h\infty}$ vs M_n only. This is demonstrated in the graph of Fig. 11.

In Fig. 11 the present data are shown by solid symbols. Other available data are shown by open symbols, including those of Rodi and Dolling,[15] Law[37] (based on data actually measured by R. D. Neumann), and Oskam et al.[38] Taken together, these data approximately describe a linear relationship within their overall scatter. The equation of the line shown in Fig. 11 is

$$\frac{C_{h_{peak}}}{C_{h\infty}} = 3.7M_n - 2.7 \tag{4}$$

This relationship is hereby proposed as a simple empirical guide for peak heating in sharp-fin-generated interactions with near-adiabatic turbulent boundary layers outboard of the inception zone near the fin leading edge. No such simple relationship is possible inside the inception zone, though the prior work of Neumann and Hayes[12] indicates lower peak heating levels there. Equation (4) would then yield a conservative estimate for practical purposes.

The data shown in Fig. 11, from which Eq. (4) is derived, are chosen from the available literature because their accuracy is reasonably documented and because it can be demonstrated that they were obtained outside the interaction inception zone. Heat transfer data at freestream Mach numbers higher than 6 are available (e.g., Ref. 39), but unfortunately this latter condition cannot be satisfied. The reason for this appears to be that very high Reynolds numbers, and consequently long distances downstream of a flat-plate leading edge, are generally required to produce an equilibrium turbulent boundary layer in hypersonic wind-tunnel testing. For this reason, such

a boundary layer tends to be comparatively thick at the location of the swept interaction, which naturally leads to a large inception zone (see Ref. 7). The dimensional limits of the hypersonic test models used so far have thus precluded the taking of data outside the inception zone.

Conclusions

This experimental study demonstrates a novel heat transfer technique for high-speed, near-adiabatic wind-tunnel testing. A foil heater generates a uniform heat flux over a flat plate surface, and miniature thin-film-resistance sensors mounted on it are used to measure the local surface temperature. The heat convection equation is then solved for the heat transfer distribution, yielding a total uncertainty of about $\pm 10\%$. The novelty of this technique lies in the use of resistance heating rather than cooling for high-speed flows, the microlithographic fabrication of the sensors, and the fact that the adiabatic wall temperature is measured rather than simply assumed to be constant. (However, results show that the adiabatic wall temperature does not vary appreciably in the present experiments, changing less than 3% across the β range of any interaction examined.)

The equilibrium turbulent boundary layer on the flat plate is subjected to impingement by swept planar shock waves generated by a sharp fin. Five different interactions with fin angles ranging from 10 to 20 deg at freestream Mach numbers of 3 and 4 produce interaction strengths from weak to very strong. The heat transfer results show a monotonic rise to a strong peak associated with the primary flow attachment line. The peak heating level varies from 2 to 5 times that of the flat plate over the range of interaction strengths studied.

These data can serve as a benchmark for CFD code validation and turbulence modeling. Accordingly, the data are compared with the results of numerical Navier-Stokes solutions that employ a k-ε turbulence model. The overall ability of the computations to predict the data is judged to be good.

Finally, a simple quasiconical correlation for the peak heat transfer in such fin interactions is suggested. This correlation demonstrates that peak heating is simply proportional to the interaction strength as expressed by the Mach number normal to the swept shock wave. The correlation is effective for near-adiabatic interactions outside the inception zone that occurs in the vicinity of the fin leading edge.

Acknowledgments

We gratefully acknowledge NASA Grant NAG 2-592, the assistance of J. D. Miller and P. Hopson Jr., and discussions with R. D. Neumann. We also appreciate the donation of materials by Alpha Wire Corp. and Cumberland Electronics, Inc.

References

[1]Horstman, C. C., "Computation of Sharp-Fin-Induced Shock Wave/Turbulent Boundary-Layer Interactions," *AIAA Journal*, Vol. 24, No. 9, 1986, pp. 1433–1440.

[2]Knight, D. D., "A Hybrid Explicit-Implicit Numerical Algorithm for the Three-Dimensional Compressible Navier-Stokes Equations," *AIAA Journal*, Vol. 22, No. 8, 1984, pp. 1056–1063.

[3]Knight, D. D., "Calculation of Three-Dimensional Shock/Turbulent Boundary-Layer Interaction Generated by a Sharp Fin," *AIAA Journal*, Vol. 23, No. 12, 1985, pp. 1885–1891.

[4]Knight, D. D., and Badekas, D., "On the Quasi-Conical Flowfield Structure of the Swept Shock Wave-Turbulent Boundary Layer Interaction," AIAA Paper 91-1759, June 1991.

[5]Knight, D., Horstman, C. C., and Settles, G. S., "Three Dimensional Shock Wave-Turbulent Boundary Layer Interactions Generated by a Sharp Fin at Mach 4," AIAA Paper 91-0648, Jan. 1991.

[6]Settles, G. S., and Dolling, D. S., "Swept Shock Wave Boundary-Layer Interactions," *Tactical Missile Aerodynamics*, edited by M. Hemsch and J. Nielsen, Vol. 104, Progress in Astronautics and Aeronautics, AIAA, New York, 1986, pp. 297–379.

[7]Settles, G. S., and Dolling, D. S., "Swept Shock/Boundary-Layer Interactions—Tutorial and Update," AIAA Paper 90-0375, Jan. 1990.

[8]Lu, F. K., "Fin Generated Shock-Wave Boundary-Layer Interactions," Ph.D. Dissertation, Mechanical Engineering Dept., Pennsylvania State Univ., University Park, PA, 1988.

[9]Kim, K.-S., Lee, Y., Alvi, F. S., Settles, G. S., and Horstman, C. C., "Laser Skin Friction Measurements and CFD Comparison of Weak-to-Strong Swept Shock/Boundary Layer Interactions," *AIAA Journal*, Vol. 29, No. 10, 1991, pp. 1643–1650.

[10]Alvi, F. S., and Settles, G. S., "Physical Model of the Swept Shock Wave/Boundary-Layer Interaction Flowfield," *AIAA Journal*, Vol. 30, No. 9, 1992, pp. 2252–2258.

[11]Hsu, J. C., and Settles, G. S., "Holographic Flowfield Density Measurements in Swept Shock Wave/Boundary-Layer Interactions," AIAA Paper 92-0746, Jan. 1992.

[12]Neumann, R. D., and Hayes, J. R., "Introduction to Aerodynamic Heating Analysis of Supersonic Missiles," *Tactical Missile Aerodynamics*, edited by M. Hemsch and J. Nielsen, Vol. 104, Progress in Astronautics and Aeronautics, AIAA, New York, 1986, pp. 421–479.

[13]Holden, M. S., "Experimental Studies of Quasi-Two-Dimensional and Three-Dimensional Viscous Interaction Regions Induced by Skewed-Shock and Swept-Shock Boundary Layer Interaction," AIAA Paper 84-1677, June 1984.

[14]Hayashi, M., Sakurai, A., and Aso, S., "Measurements of Heat-Transfer Coefficients in the Interaction Regions Between Oblique Shock Waves and Turbulent Boundary Layers with a Multi-Layered Thin Film Heat Transfer Gage," *Transactions of the Japan Society for Aeronautical Space Sciences*, Vol. 30, No. 88, Aug. 1987, pp. 102–110.

[15]Rodi, P. E., and Dolling, D. S., "An Experimental/Computational Study of Sharp Fin Induced Shock Wave/Turbulent Boundary Layer Interactions at Mach 5: Experimental Results," AIAA Paper 92-0749, Jan. 1992.

[16]Schultz, D. J., and Jones, T. V., "Heat Transfer Measurements in Short-Duration Hypersonic Facilities," AGARD-AG-165, Feb. 1973.

[17]Moody, H. L., and Jechel, K., "Heat Transfer Measurements in Cold Wind Tunnels," Air Force Wright Aeronautical Labs, AFWAL-TR-81-3176, Wright-Patterson AFB, OH, Sept. 1982.

[18]Neumann, R. D., "Aerothermodynamic Instrumentation," AGARD (to be published).

[19]Thompson, W. P., "Heat Transfer Gages," *Methods of Experimental Physics: Fluid Dynamics*, Vol. 18B, Academic Press, New York, 1981, pp. 663–685.

[20]Epstein, A. H., Guenette, G. R., Norton, R. J. G., and Yuzhang, C., "High-Frequency Response Heat-Flux Gage," *Review of Scientific Instruments*, Vol. 57, No. 4, 1986, pp. 639–649.

[21]Johnson, C. B., Carraway, D. L., Hopson, P., Jr., and Tran, S. Q., "Status of a Specialized Boundary Layer Transition Detection System for Use in the U.S. Natl. Transonic Facility," *International Congress on Instrumentation in Aerospace Simulation Facilities Record*, IEEE, New York, 1987,pp. 141–155.

[22]Simonich, J. C., and Moffat, R. J., "New Technique for Mapping Heat-Transfer Coefficient Contours," *Review of Scientific Instruments*, Vol. 53, No. 5, 1982, pp. 678–683.

[23]Hippensteele, S. A., Russell, L. M., and Stepka, F. S., "Evaluation of a Method for Heat Transfer Measurements and Thermal Visualization Using a Composite of a Heater Element and Liquid Crystals," *Journal of Heat Transfer*, Vol. 105, No. 1, 1983, pp. 184–189.

[24]Abuaf, N., Urbaetis, S. P., and Palmer, O. F., "Convection Thermography," General Electric Co., Technical Report 85CRD168, Sept. 1985.

[25]Eibeck, P. A., and Eaton, J. K., "An Experimental Investigation of the Heat Transfer Effects of a Longitudinal Vortex Embedded in a Turbulent Boundary Layer," Thermosciences Division, Dept. of Mechanical Engineering, Stanford Univ., Rept. MD-48, Stanford, CA, Nov. 1985.

[26]Lee, Y., "Heat Transfer Measurements in Swept Shock Wave/Turbulent Boundary-Layer Interactions," Ph.D. Dissertation, Mechanical Engineering Dept., Penn State Univ., University Park, PA, June 1992.

[27]Johnson, C. B., and Adcock, J. B., "Measurement of Recovery Temperature on an Airfoil in the Langley 0.3m Transonic Cryogenic Wind Tunnel," AIAA Paper 81-1062, June 1981.

[28]Mack, L. M., "An Experimental Investigation of the Temperature Recovery Factor," Jet Propulsion Lab., California Inst. of Technology, Rept. 20-80, Pasadena, CA, Aug. 1954.

[29]Stalder, J. R., Rubesin, M. W., and Tendeland, T., "A Determination of the Laminar-, Transitional-, and Turbulent Boundary

Layer Temperature Recovery Factors on a Flat Plate in Supersonic Flow," NACA TN 2077, June 1950.

[30]Coleman, H. W., and Steele, W. G., *Experimentation and Uncertainty Analysis for Engineers*, Wiley, New York, 1989.

[31]Settles, G. S., Horstman, C. C., and McKenzie, T. M., "Flowfield Scaling of a Swept Compression Corner Interaction—A Comparison of Experiment and Computation," AIAA Paper 84-0096, Jan. 1984.

[32]Jones, W. P., and Launder, B. E., "The Prediction of Laminarization with a Two-Equation Model of Turbulence," *International Journal of Heat and Mass Transfer*, Vol. 15, No. 2, 1972, pp. 301–314.

[33]Knight, D. D., Horstman, C. C., Shapey, B., and Bogdonoff, S. M., "Structure of Supersonic Flow Past a Sharp Fin," *AIAA Journal*, Vol. 25, No. 10, 1987, pp. 1331–1337.

[34]Knight, D. D., Badekas, D., Horstman, C. C., and Settles, G. S., "Quasiconical Flowfield Structure of the Three-Dimensional Single Fin Interaction," *AIAA Journal*, Vol. 30, No. 12, 1992, pp. 2809–2816.

[35]Horstman, C. C., "Hypersonic Shock-Wave/Turbulent-Boundary-Layer Interaction Flows," *AIAA Journal*, Vol. 30, No. 6, 1992, pp. 1480, 1481.

[36]Wilcox, D. C., "Program EDDYBL User's Guide," DCW Industries, Rept. DCW-R-NC-04, La Cañada, CA, Nov. 1988.

[37]Law, C. H., "3-D Shock Wave-Turbulent Boundary Layer Interactions at Mach 6," U.S. Air Force Aeronautical Research Labs, ARL TR 75-0191, Dayton, OH, June 1975; see also Christophel, R. G., and Rockwell, W. A., "Tabulated Mach 6 3-D Shock Wave-Turbulent Boundary Layer Interaction Heat Transfer Data (Supplement)," Air Force Flight Dynamics Lab, AFFDL-TM-74-212-FXG-Supplement, Dayton, OH, Nov. 1975.

[38]Oskam, B., Vas, I. E., and Bogdonoff, S. M., "Oblique Shock Wave/Turbulent Boundary Layer Interactions in Three Dimensions at Mach 3, Part 2," Air Force Flight Dynamics Lab, AFFDLTR-76-48, Pt. II, Dayton, OH, 1976.

[39]Kussoy, M. I., and Horstman, K. C., "Documentation of Two- and Three-Dimensional Shock-Wave/Turbulent-Boundary-Layer Interaction Flows at Mach 8.2," NASA TM 103838, May 1991.